Cortical *Foxp2* supports behavioral flexibility and developmental dopamine D1 receptor expression

Marissa Co, Stephanie L. Hickey, Ashwinikumar Kulkarni, Matthew Harper, Genevieve Konopka*

Department of Neuroscience, University of Texas Southwestern Medical Center, Dallas, TX, USA
*Correspondence: Genevieve.Konopka@utsouthwestern.edu

Contact information
Genevieve Konopka, Ph.D.
Department of Neuroscience, University of Texas Southwestern Medical Center,
5323 Harry Hines Blvd., ND4.300, Dallas, TX 75390-9111
TEL: 214-648-5135, FAX: 214-648-1801,
Email: Genevieve.Konopka@utsouthwestern.edu

Abstract

FoxP2 encodes a forkhead box transcription factor required for the development of neural circuits underlying language, vocalization, and motor-skill learning. Human genetic studies have associated *FOXP2* variation with neurodevelopmental disorders (NDDs), and within the cortex, it is coexpressed and interacts with other NDD-associated transcription factors. Cortical *Foxp2* is required in mice for proper social interactions, but its role in other NDD-relevant behaviors and molecular pathways is unknown. Here, we characterized such behaviors and their potential underlying cellular and molecular mechanisms in cortex-specific *Foxp2* conditional knockout mice. These mice showed deficits in reversal learning without increased anxiety or hyperactivity. In contrast, they emitted normal vocalizations save for a decrease in loudness of neonatal calls. These behavioral phenotypes were accompanied by decreases in cortical dopamine D1 receptor (D1R) expression at neonatal and adult stages, while general cortical development remained unaffected. Finally, using single-cell transcriptomics, we identified neonatal D1R-expressing cell types in frontal cortex and found changes in D1R cell type composition and gene expression upon cortical *Foxp2* deletion. Together these data support a role for *Foxp2* in the development of dopamine-modulated cortical circuits potentially relevant to NDDs.

Introduction

FoxP2 encodes a forkhead box transcription factor required for proper brain development across species, particularly in neural circuits underlying vocalization and motor-skill learning (French and Fisher 2014; Konopka and Roberts 2016). In humans, *FOXP2*-related disorders are characterized by childhood apraxia of speech, an impairment of motor programming, as well as additional motor and cognitive deficits related to language (Morgan et al. 2017; Schulze et al. 2017). Some *FOXP2* mutations are associated with autism spectrum disorder (ASD) involving social communication impairments (Reuter et al. 2017). In addition, a recent large genome-wide meta-analysis identified *FOXP2* among twelve loci associated with attention deficit/hyperactivity disorder (ADHD), a condition with shared genetic underpinnings with ASD (Ghirardi et al. 2017; Demontis et al. 2019). Thus, *FOXP2* subserves neural functions impaired across neurodevelopmental disorders (NDDs).

Cortical functions of FoxP2 may be particularly relevant to these NDDs. In mice, Foxp2 expression is restricted to layer 6 corticothalamic projection neurons and a subset of layer 5 projection neurons, cell types associated with genetic risk for ASD (Hisaoka et al. 2010; Willsey et al. 2013; Chang et al. 2015; Sorensen et al. 2015). Within these cell types, FoxP2 interacts with other NDD-associated transcription factors, such as TBR1, suggesting shared regulation of transcriptional networks by these proteins (Hisaoka et al. 2010; Deriziotis et al. 2014; Estruch et al. 2018). Importantly, cortex-specific *Foxp2* deletion causes altered social behaviors and vocalizations in adult mice, possibly through dysregulated expression of the ASD candidate gene *Mint2* (Medvedeva et al. 2018). Foxp2 also represses the language-related gene *Srpx2* in cortical neuron cultures to

regulate spine density (Sia et al. 2013). It is unknown whether loss of cortical *Foxp2* causes additional NDD-relevant behavioral deficits or dysregulated molecular pathways.

In this study, we characterized NDD-relevant behaviors and their potential underlying cellular and molecular mechanisms in cortex-specific *Foxp2* conditional knockout mice (*Emx1-Cre; Foxp2*$^{flox/flox}$). We show that this deletion impaired frontal cortex-mediated cognitive behaviors while sparing other NDD-associated behaviors, such as vocal communication and hyperactivity. Using immunohistochemistry and genetic reporter mice, we found grossly normal cortical development upon *Foxp2* deletion but decreased expression of cortical dopamine D1 receptors at neonatal and adult stages. Last, using single-cell transcriptomics, we characterized neonatal D1 receptor-expressing neuronal subtypes and identified the effects of *Foxp2* deletion on neuronal subtype composition and gene expression. Together these data support a role for *Foxp2* in the development of dopamine-modulated cortical circuits potentially relevant to cognitive impairments seen in NDDs.

Results

Cortical *Foxp2* deletion impairs behavioral flexibility

We generated cortex-specific *Foxp2* conditional knockout (cKO) mice and control littermates by crossing *Foxp2*$^{flox/flox}$ mice (French et al. 2007) with mice expressing *Emx1*-Cre, which induces recombination in progenitors and projection neurons derived from dorsal telencephalon (Gorski et al. 2002) (Fig. 1A). We confirmed absence of Foxp2 protein in the cortex and normal expression in other brain regions of adult cKO mice; we also confirmed lack of Foxp2 in control hippocampus (Supplemental Fig. 1), where *Emx1*-

Cre is also expressed. We observed no gross abnormalities in brain morphology of cKO mice (Supplemental Fig. 1), consistent with a previous study utilizing the same conditional knockout strategy (French et al. 2018).

We evaluated the contribution of cortical *Foxp2* to NDD-relevant behaviors, such as behavioral flexibility, hyperactivity, anxiety, and ultrasonic vocalizations (USVs). To assess behavioral flexibility in *Foxp2* cKO mice, we utilized a water Y-maze assay and found significant deficits in reversal learning, but not initial acquisition, of escape platform location (Fig. 1B-C, statistics for behavioral testing are provided Supplemental Table 1). As an additional assay of frontal cortical function, we assessed spontaneous alternation in a dry T-maze (Lalonde 2002). While there were no significant differences between genotypes in alternation rate or latency to arm, control mice alternated significantly above chance levels while cKO mice did not (Supplemental Fig. 2A-B, Supplemental Table 1).

We performed additional assays to determine whether locomotor or anxiety phenotypes contributed to *Foxp2* cKO impairment in these cognitive tasks. There were no differences in baseline activity levels in a novel cage (Supplemental Fig. 2C, Supplemental Table 1) or total distance moved in an open field (Supplemental Fig. 2D, Supplemental Table 1). Furthermore, each genotype spent equal amounts of time in the center or open arms of the open field or elevated plus maze, respectively, indicating normal anxiety levels in cKO mice (Supplemental Fig. 2E-F, Supplemental Table 1). Altogether these data indicate that cortical *Foxp2* is required for behavioral flexibility in mice.

Cortical *Foxp2* deletion decreases sound pressure of neonatal vocalizations

Adult male mice with cortical *Foxp2* deletion using *Nex*-Cre show subtle abnormalities in courtship USVs (Medvedeva et al. 2018); therefore, we investigated courtship USV production and spectral features in our *Emx1*-Cre *Foxp2* cKO mice. Using automated call detection methods (Holy and Guo 2005), we found no differences between genotypes in measures related to call number, timing, structure, pitch, or intensity (Fig. 1D, Supplemental Table 1). We next used an automated method to cluster calls into 100 call types (repertoire units or RUs) and compare repertoires between genotypes (Van Segbroeck et al. 2017) (Fig. 1E-F and Supplemental Fig. 2G). This yielded a similarity matrix comparable to matrices generated between cohorts of wild-type C57BL/6 mice (Van Segbroeck et al. 2017), with the top 74 of 100 RUs having Pearson correlations greater than 0.8 (Fig. 1E). Because the similarity matrix does not account for frequency of call types used, we calculated a median (top 50% most used RUs) similarity score of 0.90 and an overall (top 95%) similarity score of 0.86 between control and cKO repertoires (Fig. 1F). Comparing this to the average similarity of 0.91 ± 0.03 between replicate C57BL/6 studies (Van Segbroeck et al. 2017) leads us to conclude that cKO mice do not differ greatly from controls in courtship call structure and usage.

Neonatal mice with whole-body *Foxp2* deletion emit fewer isolation USVs (Shu et al. 2005), so we investigated the contribution of cortical *Foxp2* to isolation USVs across postnatal development (P4, P7, P10, P14). Again, we found no differences between genotypes in measures related to call number, timing, structure, or pitch (Fig. 1G, Supplemental Table 1). There was, however, a small but significant decrease in the relative sound pressure of calls emitted by *Foxp2* cKO pups across development (Fig. 1G, Supplemental Table 1). This decrease in loudness was not due to somatic weakness,

as cKO pups gained weight and performed gross motor functions normally (Supplemental Fig. 2H-J, Supplemental Table 1). In summary, cortical *Foxp2* plays a specific role in loudness of neonatal vocalizations, but not in production or other acoustic features of neonatal or adult vocalizations.

Cortical *Foxp2* is dispensable for lamination and layer 6 axon targeting

We asked whether cortical anatomical abnormalities could underlie the cognitive deficits in *Foxp2* cKO mice. Because knockdown of *Foxp2* in embryonic cortex impairs neuronal migration (Tsui et al. 2013), we examined cortical layering in cKO mice using DAPI staining of cytoarchitecture and immunohistochemistry for layer markers CUX1 (L2-4), CTIP2 (L5b) and TBR1 (L6). We found no gross abnormalities in layer formation or relative thickness at P7 (Supplemental Fig. 3A-B, all numbers and statistics for immunohistochemistry are provided Supplemental Table 1). Next, because Foxp2 regulates genes involved in neurite outgrowth in the embryonic brain (Vernes et al. 2011), we examined the formation of cortical L6 axon tracts labeled with *golli*-τ-eGFP in P14 cKO mice (Jacobs et al. 2007) (Supplemental Fig. 3C). We observed no qualitative differences in L6 axon tracts throughout the brain (including the internal capsule, which contains corticothalamic axons), innervation of thalamic nuclei, or intra-cortical axon projections to L4 (Supplemental Fig. 3D). These results show that *Foxp2* deletion from cortical progenitors and neurons does not affect gross cortical layering or targeting of L6 axons.

***Foxp2* deletion reduces cortical dopamine D1 receptor expression**

We next explored the possibility that Foxp2 activates expression of the dopamine D1 receptor (D1R) in L6 corticothalamic projection neurons (CThPNs), as inhibition of D1-like receptors or L6 CThPN activity in the frontal cortex impairs reversal learning

(Calaminus and Hauber 2008; Nakayama et al. 2018). Retrograde labeling in rodents has shown that L6 CThPNs express Foxp2 or D1R (Gaspar et al. 1995; Sorensen et al. 2015), but no studies to date have shown colocalization of these proteins in the cortex. However, D1R expression is enriched in Foxp2+ neurons of the mouse striatum and decreased in the zebra finch striatum upon *FoxP2* knockdown (Vernes et al. 2011; Murugan et al. 2013). Thus, we hypothesized that Foxp2 also activates D1R expression in mouse L6 CThPNs.

To visualize D1R expression, we crossed our *Foxp2* cKO mice with *Drd1a*-tdTomato reporter mice, which replicate endogenous *Drd1* expression patterns in the cortex (Ade et al. 2011; Anastasiades et al. 2018) (Fig. 2A). We observed fewer D1R+ cells throughout the frontal cortex of adult cKO mice (Fig. 2B), but Foxp2 and D1R were not expressed in the same cellular subpopulation in control L6 (Fig. 2C). Adult mouse L6 contains *Foxp2*+ CThPNs and *Foxp2*- intratelencephalic projection neurons (ITPNs) (Sorensen et al. 2015; Anastasiades et al. 2018), so our result indicates that adult mouse L6 D1R+ neurons are predominantly ITPNs, and that early *Foxp2* deletion causes lasting reductions in ITPN D1R expression. Because D1-like receptor density undergoes developmental pruning in PFC (Andersen et al. 2000), we asked whether early postnatal CThPNs express D1R, and whether *Foxp2* deletion decreases D1R in postnatal cortex. In contrast with adult cortex, postnatal cortex showed extensive coexpression of Foxp2 and D1R in L6 (Fig. 2D), and we again saw a reduction of D1R+ cells throughout the frontal cortex of cKO mice (Fig. 2E). Quantification of D1R+ cells in the medial prefrontal cortex (mPFC) revealed significant reductions in L5 and L6, where Foxp2 expression normally occurs (Fig. 2F-G, Supplemental Table 1).

Loss of D1R in postnatal *Foxp2* cKO cortex could result from either decreased number of CThPNs or downregulation of D1R expression within these cells. We examined the CThPN marker TLE4 (Molyneaux et al. 2015) and its coexpression with Foxp2 and/or D1R in control mPFC, and found a high degree of overlap among the three proteins in L6 and a moderate degree of overlap in L5 (Fig. 2H-I, Table 1). We found no differences in the percentage of TLE4+ cells in L5 or L6 between genotypes (Fig. 2J, Table 1). Instead, we found significant reductions in the percentage of TLE4+ neurons expressing D1R in cKO mice (Fig. 2I, Table 1). These results agree with the finding of unaltered neuronal density in L5-6 of adult mice lacking *Foxp2* through the same conditional knockout strategy (French et al. 2018). Interestingly, although nearly all (~92%) control TLE4+ neurons were Foxp2+/D1R+, ~41% of TLE4+ neurons still maintained D1R expression after *Foxp2* deletion (Fig. 2I, Table 1), suggesting that *Foxp2* is not required in all CThPNs for expression of D1R. To summarize, cortical *Foxp2* deletion does not affect TLE4+ CThPN number or identity but reduces D1R expression in postnatal CThPNs and adult ITPNs.

Identification of D1R-expressing cell types in developing frontal cortex

Studies using retrograde labeling and genetic markers have identified excitatory and inhibitory neuronal subtypes expressing D1R in adult mouse mPFC (Han et al. 2017; Anastasiades et al. 2018), but less is known about cell types expressing D1R in postnatal cortex. To identify these cell types and understand cell type-specific alterations upon *Foxp2* deletion, we used fluorescence-activated cell sorting (FACS) followed by single-cell RNA sequencing (scRNA-seq) to genetically profile *Drd1a*-tdTomato+ frontal cortical neurons from P7 control and *Foxp2* cKO mice (Fig. 3A). Using the 10x Genomics

Chromium platform (Zheng et al. 2017), we profiled a total of 7282 cells from 2 mice per genotype, and we detected similar numbers of transcripts and genes between genotypes and among mice (Supplemental Fig. 4A). Using Seurat (Butler et al. 2018) we identified 21 clusters, each of which contained cells from all mice examined (Supplemental Fig. 4B-C, Supplemental Table 2). To annotate cell types, we overlapped our cluster marker genes with markers from a P0 cortical scRNA-seq dataset (Loo et al. 2019), and found significant overlaps with neuronal, astrocyte, oligodendrocyte, and endothelial clusters (Supplemental Fig. 4D). We confirmed this analysis by examining expression of canonical marker genes for each cell type (Supplemental Fig. 4E). While *Drd1* was not expressed in every cell, it was expressed in every cluster, and re-clustering *Drd1*+ cells resulted in similar cell types as the full dataset (Supplemental Fig. 4E-G, Supplemental Table 2). As *tdTomato* transcripts are roughly double that of *Drd1* in individual cells of *Drd1a*-tdTomato mouse cortex (Anastasiades et al. 2018), these results suggest that FACS isolated tdTomato+ cells for which we could not detect *Drd1* transcripts by scRNA-seq. Furthermore, *Drd1* transcripts appear to be present in both neurons and glia of the developing frontal cortex, supporting evidence for expression and activity of D1-like receptors in prefrontal cortical astrocytes (Vincent et al. 1993; Liu et al. 2009).

To refine our D1R neuronal subtype classification, we reclustered the neuronal clusters and identified 11 clusters comprised of 2758 cells (Fig. 3B, Supplemental Table 2). Two low-quality clusters (Clusters 2, 7) were excluded from further assessments, and annotation of the remaining clusters based on P0 data revealed multiple subclasses of upper- and lower-layer projection neurons and interneurons (Loo et al. 2019) (Fig. 3C). To delineate projection neuron clusters by their projection specificity, we also examined

expression of marker genes from a scRNA-seq dataset with retrograde labeling in adult frontal motor cortex (Tasic et al. 2018) (Fig. 3D). We were able to distinguish L6 CThPNs by *Foxp2, Tle4,* and *Ephb1* (Cluster 4), L5 near-projecting neurons (NPNs) by *Trhr* and *Tshz2* (Cluster 9), L6 ITPNs by *Oprk1* (Cluster 10), and L2/3 ITPNs by *Mdga1* and *Pou3f1* (Cluster 3). Cluster 0 may contain a mix of L2/3 and L5 ITPNs as indicated by expression of both *Pou3f1* and the L5 ITPN marker *Rorb*. Notably, *Foxp2* expression in postnatal projection neurons was restricted to non-ITPNs, suggesting that the loss of D1R in ITPNs of *Foxp2* cKO adult mice may be a non-cell-autonomous effect (Fig. 2B-C, Fig. 3D). We also distinguished interneuron subtypes in our scRNA-seq data by expression of *Htr3a* (Cluster 1), *Lamp5* (Cluster 6), and *Sst* (Cluster 8). These results reveal an unprecedented diversity of D1R-expressing projection neuron and interneuron subtypes in the developing frontal cortex.

Foxp2 **deletion increases SP9+ interneuron numbers in postnatal cortex**

Given that postnatal *Foxp2* cKO mice show reduced D1R expression in CThPNs, but by adulthood show reduced D1R expression in ITPNs, we asked if this non-cell-autonomous effect was occurring during development by examining the proportion of cKO cells in each D1R neuronal cluster. We found significant underrepresentation of cKO cells in L6 CThPN and L2/3 ITPN clusters, and overrepresentation in interneuron Cluster 5 (Fig. 3E). Cluster 5 overlapped significantly with a P0 cluster representing migrating cortical interneurons, and expressed high levels of *Cdca7* and *Sp9* while expressing lower levels of mature interneuron subtype markers (Loo et al. 2019) (Fig. 3C-D). Cluster 5 also expressed *Foxp2*, suggesting it arises from an *Emx1*-negative lineage such as basal forebrain-derived cortical interneurons (Gorski et al. 2002) (Fig. 3D).

Immunohistochemistry for SP9 in *Drd1a*-tdTomato *Foxp2* cKO mPFC confirmed this increase in total SP9+ cells as well as SP9+D1R+ cells upon *Foxp2* deletion (Fig. 3F-G, Supplemental Table 1). Thus, in postnatal frontal cortex, loss of *Foxp2* in *Emx1*-positive cells causes non-cell-autonomous effects on ITPN D1R expression and cortical interneuron development.

Foxp2 deletion induces non-cell-autonomous effects on cortical gene expression

To elucidate molecular pathways in cortical D1R neurons affected by *Foxp2* deletion, we performed “pseudo-bulk RNA-seq” differential gene expression analyses between genotypes in our scRNA-seq data. First, we identified differentially expressed genes between all control neurons and all *Foxp2* cKO neurons and found 48 downregulated and 35 upregulated genes in cKO neurons (Fig. 4A, Supplemental Table 3). Overlap of these DEGs with our neuronal cluster markers revealed enrichment of downregulated genes in projection neurons and enrichment of upregulated genes in interneurons (Fig. 4B). Gene ontology (GO) analyses of downregulated genes suggested abnormal synaptic plasticity, catecholamine signaling, and microtubule-based processes in cKO projection neurons, while upregulated GO terms were consistent with the increased immature interneurons seen in cKO cortex (Fig. 4C, Supplemental Table 4). We confirmed some of these DEGs in an independent scRNA-seq dataset generated from P7 control and cKO mice expressing the *golli*-τ-eGFP reporter, expression of which was not decreased in cKO cortex (Supplemental Fig. 3D, Supplemental Fig. 5, Supplemental Table 3). This suggests that the differential gene expression findings in our *Drd1a*-tdTomato dataset are not entirely due to uneven sampling of control and cKO tdTomato+ neurons across clusters (Figure 3E).

In a more cell type-specific approach, we also identified DEGs between genotypes by neuronal cluster in the *Drd1a*-tdTomato dataset (Fig. 4D, Supplemental Table 5). CThPNs in cKO mice had few gene expression changes but showed downregulation of *Ppp1r1b*, which encodes the D1R downstream signaling protein DARPP-32 and is directly bound by Foxp2 at its promoter (Vernes et al. 2011) (Fig. 4E). In contrast, ITPN clusters had more DEGs, and GO analysis identified cytoskeletal genes among the downregulated genes of cKO L2-5 ITPNs (Fig. 4E). The relatively small number of DEGs in *Foxp2*-expressing CThPNs and NPNs was not due to upregulation of related genes *Foxp1* or *Foxp4* (Fig. 4F). Additionally, both 5-HT3R and LAMP5 interneurons downregulated *Fos* and upregulated the organic ion transporter *Slc22a15* in response to cortical *Foxp2* deletion, while SST interneurons downregulated *Npy* and *Gap43* (Fig. 4E). In summary, while *Foxp2* expression is restricted to deep-layer non-ITPNs, its deletion causes cytoskeletal gene downregulation in upper-layer ITPNs and additional non-cell-autonomous changes in interneurons.

Putative direct targets of Foxp2 in postnatal cortex

Last, to identify Foxp2 targets in a manner uninfluenced by altered D1R neuronal composition in *Foxp2* cKO cortex, we searched for genes correlated (i.e. activated) or anticorrelated (i.e. repressed) with *Foxp2* expression across control neurons in the *Drd1a*-tdTomato dataset (Fig. 4G, Supplemental Table 6). To identify potential direct targets, we overlapped these genes with targets from a Foxp2 promoter-binding assay performed in embryonic mouse brain (Vernes et al. 2011). Finally, to determine their cell type-specificity, we overlapped these putative direct Foxp2 targets with our neuronal cluster markers (Fig. 4H). We found shared and distinct Foxp2-activated targets between

CThPNs and NPNs, several of which may exert non-cell-autonomous effects through extracellular matrix organization (*Col23a1, P4ha1*), cell-cell signaling (*Islr2, Plxna2, Sdk1*), or synaptic activity (*Cacna1a, Calm2, Cbln1, Grm3, Lrrtm2*) (Fig. 4H). We also identified Foxp2-repressed targets, which were markers for ITPNs, interneurons, and CR cells, suggesting that Foxp2 plays a role in repressing these identities in CThPNs and NPNs (Fig. 4H). These results provide potential mechanisms by which Foxp2 may exert non-cell-autonomous effects and contribute to the maintenance of deep-layer cortical projection neuron identity.

Discussion

Foxp2-regulated cortical dopamine signaling and behavioral flexibility

We have demonstrated a requirement for *Foxp2* in frontal cortex-mediated behavioral flexibility and proper cortical dopamine D1R expression throughout the postnatal lifespan (Fig. 5). Moreover, we identified unexpected non-cell-autonomous alterations in D1R neuronal composition and gene expression upon cortical *Foxp2* deletion (Fig. 5). Given that cortical D1R signaling can regulate reversal learning and many other cognitive functions (Calaminus and Hauber 2008; Mizoguchi et al. 2009; Mizoguchi et al. 2010; Floresco 2013), it is plausible that the behavioral deficits in *Foxp2* cKO mice arise from their D1R neuronal abnormalities. Another form of behavioral flexibility, strategy set-shifting, may also depend on Foxp2-mediated cortical D1R circuit function. For example, humanized *Foxp2* mice show faster transitioning from place-based to response-based learning in a T-maze, as well as altered frontal cortical dopamine concentrations and corticostriatal physiology (Enard et al. 2009; Schreiweis et al. 2014).

The ability to switch between strategies in this task requires proper *Drd1* expression in the mPFC and intact corticostriatal signaling (Cui et al. 2018). Because we see altered D1R expression in ITPNs of adult *Foxp2* cKO mice, they may also exhibit altered corticostriatal signaling and strategy set-shifting ability.

Abnormal D1R signaling could also contribute to the increased migrating or immature interneurons in postnatal *Foxp2* cKO cortex, as D1 receptor modulation regulates cortical interneuron migration in embryonic forebrain slice preparations (Crandall et al. 2007). Contribution of cortical dopamine signaling to this process may explain the abnormal neuronal migration after cortical *Foxp2* knockdown at E13/14, when Foxp2-expressing projection neurons have already reached the cortical plate and are positioned to influence interneuron migration through D1R regulation (Tsui et al. 2013). Alternatively, altered dopamine sensitivity of *Foxp2* cKO excitatory projection neurons may prevent the activity-dependent apoptosis of these interneurons, which normally occurs around the postnatal time point examined in our study (Lim et al. 2018). Integration of these excess interneurons into cortical circuits could then impair circuit function and lead to behavioral deficits.

Recent human genetic studies suggest that *FOXP2* variation is associated with ASD and ADHD (Reuter et al. 2017; Demontis et al. 2019; Satterstrom et al. 2019). Genetic perturbations of dopamine signaling have also been implicated in NDDs (Money and Stanwood 2013), and NDD mouse models commonly show dopaminergic dysfunction (Robinson and Gradinaru 2018). Notably, *Foxp2* cKO mice phenocopy the decreased cortical dopamine gene expression (*Drd1*, *Ppp1r1b*) and reversal learning impairments seen in 16p11.2 and *Tbr1* mouse models of ASD (Huang et al. 2014;

Portmann et al. 2014; Yang et al. 2015), suggesting a convergent phenotype of dysregulated cortical D1R signaling in NDDs affecting behavioral flexibility. Also, because FOXP2 and TBR1 interact, these dopamine-related genes may be candidate co-regulated targets of these transcription factors (Deriziotis et al. 2014).

Roles of cortical Foxp2 in mouse vocalization

Mice with *Foxp2* mutations commonly exhibit USV abnormalities (French and Fisher 2014; Castellucci et al. 2016; Chabout et al. 2016; Gaub et al. 2016), which have been attributed to its functions in the striatum (Chen et al. 2016), cerebellum (Fujita-Jimbo and Momoi 2014; Usui et al. 2017b), and laryngeal cartilage (Xu et al. 2018). Cortical *Foxp2* deletion using *Nex*-Cre was previously shown to alter adult USVs in a social context-dependent manner (Medvedeva et al. 2018), but in our study, *Emx1*-Cre-mediated deletion did not appear to impact adult courtship USVs. *Nex*-Cre causes recombination around embryonic day (E) 11.5 in postmitotic projection neurons, whereas *Emx1*-Cre acts by E10.5 in both projection neurons and their progenitors (Gorski et al. 2002; Goebbels et al. 2006). Thus, perhaps earlier deletion of *Foxp2* from the cortex induces developmental compensation in vocalization circuitry that cannot occur after postmitotic neuronal deletion. We also did not classify calls based on duration, direction, or size of pitch jumps as did the previous study, but our call repertoire analysis suggested high overall similarity between control and cKO vocalizations. Other methodological differences, such as testing environment or ovulation state of female mice, may also differentially affect USV results between studies.

Neonatal isolation USVs were also largely unaffected by loss of cortical *Foxp2*, contrasting with the USV reductions in pups with cortical *Foxp1* deletion or cerebellar

Foxp2 knockdown (Usui et al. 2017a; Usui et al. 2017b). Whereas Foxp2 is expressed in CThPNs, Foxp1 is likely expressed in callosal and corticostriatal neurons based on its coexpression with Satb2 (Hisaoka et al. 2010; Sohur et al. 2014; Sorensen et al. 2015). Furthermore, cortical layering is altered in *Foxp1* cKO but not *Foxp2* cKO mice (Usui et al. 2017a). Thus, proper positioning and function of ITPNs and cerebellar output neurons may be more essential to USV production than CThPNs.

Cortical *Foxp2* deletion did decrease the sound pressure of USVs across postnatal development. Homozygous *Foxp2-R552H* mutant pups also emit quieter ultrasonic distress calls, which correlates with overall developmental delay of mutants (Groszer et al. 2008; Gaub et al. 2010). However, cortical *Foxp2* alone at least partly contributes to call loudness, as our cKO pups showed grossly normal development. By adulthood, heterozygous *Foxp2-R552H* mutants emit abnormally loud courtship USVs and show ectopic positioning of L5 laryngeal motor cortex neurons (Chabout et al. 2016; Gaub et al. 2016). Whether this neuronal population is altered in *Foxp2* cKO pups and contributes to call loudness remains to be explored.

Gene expression regulation by Foxp2 in the cortex

Single-cell RNA-seq permitted the use of complementary approaches for identifying gene expression programs regulated by Foxp2 in postnatal frontal cortex. Identifying DEGs between genotypes regardless of neuronal subtype allowed us to assess general dysregulated biological processes in cKO D1R neurons, such as downregulated synaptic plasticity and upregulated cell immaturity. Identifying DEGs by neuronal subtype led to an unexpected finding of large gene expression changes in *Foxp2*-negative ITPNs, such as downregulated cytoskeletal genes. Finally, overlapping

Foxp2-correlated genes with brain-wide direct Foxp2 targets revealed putative cortical direct targets, which may not have appeared among DEGs because of *Drd1a*-tdTomato sampling bias, small effect sizes, or compensatory mechanisms for gene regulation.

Several Foxp2-regulated genes are of interest due to their connection with NDDs. Overlap of direct targets with *Tbr1* knockout DEGs reveals potential co-activated (*Adcy1*, *Cbln1*, *Grm3*, *Lrrtm2*, *Nfe2l3*, *Nfia*, *Nin*, *Sdk1*, *Ppp1r1b*, *Sox5*) and co-repressed (*Inhba*) genes by Foxp2-TBR1 interaction (Bedogni et al. 2010; Vernes et al. 2011; Deriziotis et al. 2014; Fazel Darbandi et al. 2018). *Foxp2* expression was anticorrelated with the ASD gene *Mef2c*, which is also repressed by Foxp2 in the striatum to control wiring of cortical synaptic inputs (Chen et al. 2016). Additionally, recently identified ADHD-associated loci include *Foxp2* as well as *Foxp2*-correlated genes *Dusp6*, *Pcdh7*, and *Sema6d*, the last of which is a direct Foxp2 target (Vernes et al. 2011; Demontis et al. 2019). We note that our direct target analysis is limited to Foxp2-bound promoters in embryonic brain (Vernes et al. 2011), and recent evidence suggests that FOXP2 promotes chromatin accessibility at enhancers to regulate gene expression in developing neurons (Hickey et al. 2019). Thus, genome-wide targets of Foxp2 must be identified at various developmental stages for a full understanding of its functions in the cortex. Nonetheless, we have identified roles for Foxp2 in the development of dopaminoceptive cortical neurons and cognitive behaviors, which carry implications for our understanding of neurodevelopmental disorders.

Materials and Methods

Mice

All procedures were approved by the Institutional Animal Care and Use Committee of UT Southwestern. *Emx1-Cre* (Gorski et al. 2002) (#005628, Jackson Laboratory), *Foxp2*$^{flox/flox}$ (French et al. 2007) (#026259, Jackson Laboratory) and *Drd1a-tdTomato* line 6 mice (Ade et al. 2011) (#016204, Jackson Laboratory, provided by Dr. Craig Powell) were backcrossed with C57BL/6J mice for at least 10 generations. Genotyping primers can be found in Supplemental Table 7. Experimental mice (*Foxp2* cKO) and control littermates were generated by crossing male *Emx1-Cre*; *Foxp2*$^{flox/flox}$ mice with female *Foxp2*$^{flox/flox}$ mice. When used, *Drd1a-tdTomato* was present in mice of either sex for breeding. Mice were group-housed under a 12 h light/dark cycle and given *ad libitum* access to food and water. Mice of both sexes were used for all experiments except adult USVs, which were measured in male mice.

Behavioral analyses

Adult *Foxp2* cKO and control littermates were tested at age 10-20 weeks, and pups were tested at postnatal days 4, 7, 10, and 14. Additional behavioral procedures can be found in the Supplemental Material.

Reversal learning in water Y-maze

Mice were tested according to (Stoodley et al. 2017) using a Y-shaped apparatus filled with 20-22°C water up to 0.5 cm above a clear movable platform. On day 1, mice were habituated to the maze for 1 min without the platform. On days 2-4 (Training 1-3), mice were given 15 trials/day, up to 30 s each, to learn the platform location in one of the maze arms. Platform location was counter-balanced by cage to control for side biases. On days

4-6 (Reversal 1-3), the platform was moved to the opposite arm and mice were given 15 trials/day to learn the new location. The fraction of correct trials per day was calculated, as well as number of trials to reach a criterion of 5 consecutive correct trials. Differences between genotypes were assessed using a two-way ANOVA with Bonferroni's multiple comparisons test.

Adult courtship ultrasonic vocalizations

Mice were tested according to (Araujo et al. 2017). Male test mice were paired with age-matched C57BL/6J females for 1 week, then single-housed for 1 week. On the test day, males were habituated in their home cages to the testing room for 30 min, during which their cage lids were replaced with Styrofoam lids containing UltraSoundGate condenser microphones (Avisoft Bioacoustics) positioned at a fixed height of 20 cm. The microphones were connected to UltraSoundGate 416H hardware (Avisoft Bioacoustics) connected to a computer running RECORDER software (Avisoft Bioacoustics). At the start of testing, an unmated age-matched C57BL/6J female was placed in each cage and resultant male songs were recorded for 3 min. Spectrogram preparation and call detection were performed using MATLAB code developed by (Rieger and Dougherty 2016) based on methods from (Holy and Guo 2005). Differences between genotypes were assessed using unpaired t-tests. Call repertoire analysis was performed using the MUPET MATLAB package (Van Segbroeck et al. 2017) with a repertoire size of 100 units.

Neonatal isolation ultrasonic vocalizations

Mice were tested according to (Araujo et al. 2015). After habituation in their home cages to the testing room for 30 min, individual pups were placed in plastic containers within 1 of 4 soundproof Styrofoam boxes with lids containing UltraSoundGate condenser

microphones. Pups were randomly assigned to recording boxes at each postnatal time point. Isolation USVs were recorded for 3 min and analyzed using the same MATLAB code used for adult USV analysis. Differences between genotypes were assessed using a two-way ANOVA with Bonferroni's multiple comparisons test.

Immunohistochemistry

Neonatal and adult mice were anesthetized (pups by cryoanesthetization, adults by injection with 80-100 mg/kg Euthasol) and transcardially perfused with 4% PFA, and their brains were post-fixed overnight in 4% PFA. After cryoprotection in 30% sucrose overnight, brains were embedded in Tissue-Tek CRYO-OCT Compound (#14-373-65, Thermo Fisher Scientific) and cryosectioned at 20-40 µm. Staining was performed on free-floating sections and all washes were performed with TBS or 0.4% Triton X-100 in TBS (TBS-T) unless otherwise stated. For TLE4 staining, antigen retrieval was performed in citrate buffer (10 mM tri-sodium citrate, 0.05% Tween-20, pH 6) for 10 min at 95°C. Free aldehydes were quenched with 0.3M glycine in TBS for 1 h at room temperature. Sections were incubated overnight at 4°C in primary antibodies diluted in 3% normal donkey serum and 10% bovine serum albumin (BSA) in TBS-T. Secondary antibody incubations were performed for 1 h at room temperature in 10% BSA in TBS-T. Sections were mounted onto slides, incubated in DAPI solution (600 nM in PBS) for 5 min at room temperature, and washed 3X with PBS. Coverslips were mounted using ProLong Diamond Antifade Mountant (#P36970, Thermo Fisher Scientific). The following antibodies and dilutions were used: rabbit α-Foxp2 (#5337S, Cell Signaling Technology, 1:250), rabbit α-SP9 (#PA564038, Thermo Fisher Scientific, 1:100), goat α-tdTomato

(#LS-C340696, LifeSpan BioSciences, 1:500), mouse α-TLE4 (#sc-365406, Santa Cruz Biotechnology, 1:200), species-specific secondary antibodies produced in donkey and conjugated to Alexa Fluor 488, Alexa Fluor 555, or Alexa Fluor 647 (Thermo Fisher Scientific, 1:2000).

Imaging and Image Analysis

Images were acquired using a Zeiss LSM 880 confocal microscope at the UT Southwestern Neuroscience Microscopy Facility and processed and analyzed using Zeiss ZEN Lite and FIJI. For cell counts, tile scan Z-stack images of the region of interest were acquired at 20X magnification from similar coronal sections across 2-3 mice/genotype. Stitched maximum intensity projection images were used for manual cell counting using the FIJI Cell Counter plugin. Layers in mPFC were defined based a combination of DAPI-based cytoarchitecture and TLE4+ cell distribution. Differences between genotypes were assessed using a two-way ANOVA with Bonferroni's multiple comparisons test.

Single-cell RNA-seq (scRNA-seq)

Tissue processing and library generation

Tissue was dissociated for scRNA-seq based on (Tasic et al. 2016). P7 mice were sacrificed by rapid decapitation and brains were quickly removed and placed in ice-cold artificial cerebrospinal fluid (ACSF) (126 mM NaCl, 20 mM $NaHCO_3$, 20 mM D-Glucose, 3 mM KCl, 1.25 mM NaH_2PO_4, 2 mM $CaCl_2$, 2 mM $MgCl_2$) bubbled with 95% O_2 and 5% CO_2. 400-µm coronal sections were made in ACSF using a VF-200 Compresstome and

transferred to a room temperature recovery chamber with ACSF containing channel blockers DL-AP5 sodium salt (50 µM), DNQX (20 µM), and tetrodotoxin (100 nM) (ACSF+). After 5 min, frontal isocortex was separated from olfactory areas, cut into smaller pieces and incubated in 1 mg/ml pronase (#P6911, Sigma-Aldrich) in ACSF+ for 5 min. Pronase solution was replaced with 1% BSA in ACSF and tissue pieces were gently triturated into single-cell suspension using polished glass Pasteur pipettes with 600 µm, 300 µm, and 150 µm openings. Cells were filtered twice through Flowmi 40 µm Cell Strainers (#H13680-0040, Bel-Art) and live, single tdTomato+ cells were sorted using a BD FACSAria (BD Biosciences) at the UT Southwestern Flow Cytometry Facility. After sorting, cells were centrifuged and resuspended in 0.04% BSA in ACSF to target 1000 cells/sample using the Chromium Single Cell 3' Library & Gel Bead Kit v2 (#120237, 10x Genomics) (Zheng et al. 2017). Tissue and library preparation were performed in the following batches: Batch 1 – D1Tom-CTL1 (F), D1Tom-CKO1 (F); Batch 2 – D1Tom-CTL2 (F), D1Tom-CKO2 (M). Libraries were sequenced using an Illumina NextSeq 500 at the McDermott Sequencing Core at UT Southwestern.

Data processing

BCL files were demultiplexed with the i7 index using Illumina's bcl2fastq v2.17.1.14 and *mkfastq* from 10x Genomics CellRanger v2.1.1. Extracted paired-end fastq files, consisting of a 26 bp cell barcode and unique molecular identifier (UMI) (R1) and a 124 bp transcript sequence (R2), were checked for read quality using FASTQC v0.11.5 (Andrews 2010). R1 reads were used to estimate and identify real cells using *whitelist* from UMI-tools v0.5.4 (Smith et al. 2017). A whitelist of cell barcodes and R2 fastq files were used to extract reads corresponding to cells using *extract* from UMI-tools v0.5.4.

This step also appended the cell barcode and UMI sequence information from R1 to read names in the R2 fastq file. Extracted R2 reads were aligned to the mouse reference genome (MM10/GRCm38p6) from the UCSC genome browser (Kent et al. 2002) and reference annotation (Gencode vM17) using STAR v2.5.2b (Dobin et al. 2013) allowing up to 5 mismatches. Uniquely mapped reads were assigned to exons using *featureCounts* from the Subread package (v1.6.2) (Liao et al. 2014). Assigned reads were sorted and indexed using Samtools v1.6 (Liao et al. 2014) and then used to generate raw expression UMI count tables using *count* from UMI-tools v0.5.4. For libraries sequenced in multiple runs, the commonly identified cell barcodes between runs were used for downstream analysis.

Clustering analysis

Cell clusters were identified using the Seurat R package (Butler et al. 2018). Individual cells were retained in the dataset based on the following criteria: <20,000 UMIs, <10% mitochondrial transcripts, <20% ribosomal protein gene transcripts. Sex chromosome and mitochondrial genes were removed from the analysis after filtering. The filtered data were log normalized with a scale factor of 10,000 using *NormalizeData*, and 1576 variable genes were identified with *FindVariableGenes* using the following parameters: mean.function = ExpMean, dispersion.function = LogVMR, x.low.cutoff = 0.2, x.high.cutoff = 2.5, y.cutoff = 0.5. Cell cycle scores were calculated using *CellCycleScoring* as per the Satija Lab cell cycle vignette (https://satijalab.org/seurat/cell_cycle_vignette.html). UMI number, percent mitochondrial transcripts, percent ribosomal protein gene transcripts, library, and cell cycle scores were regressed during scaling. Using JackStraw analysis, we selected principal components (PCs) 1-47 for clustering, excluding PCs with >1

immediate early gene (IEG) in the top 30 associated genes. We used a resolution of 1.6 for UMAP clustering and *ValidateClusters* with default parameters did not lead to cluster merging.

Cell type annotation

Cluster marker genes were identified using *FindAllMarkers* with default parameters. Clusters were broadly annotated by enriched expression of canonical marker genes (e.g. Astrocytes: *Aqp4*; Microglia: *P2ry12*; Neurons: *Rbfox1*; Excitatory neurons: *Slc17a7*; Layer 2-4 neurons: *Satb2*; L5-6 neurons: *Fezf2*; L1 neurons: *Lhx5*; Interneurons: *Gad1*; Oligodendrocytes: *Sox10*). We refined these annotations by comparing our cluster markers with markers from a published scRNA-seq dataset from P0 mouse cortex (Loo et al. 2019). Metadata and raw expression values for this dataset were downloaded from https://github.com/jeremymsimon/MouseCortex. Cells were filtered as in the original publication and expression values normalized using Seurat's *NormalizeData* with default parameters. The cluster identity of each cell was imported from the published metadata and cluster marker genes were identified using *FindAllMarkers* in Seurat. Enrichment of significant P0 marker genes (adj $p<0.05$) among our P7 cluster marker genes was analyzed using hypergeometric testing with a background of 2800 genes (the average of the median number of expressed genes in each cluster). P values were corrected for multiple comparisons using the Benjamini-Hochberg procedure.

Neuronal re-clustering, annotation, and gene expression analyses

Cells belonging to neuronal clusters (Clusters 2, 6, 8, 10-12, 14-17 in Supplemental Fig. 4B) were pulled from the full dataset and re-clustered with resolution 1.2 and PCs 1-59, excluding PCs with >1 IEG in the top 30 associated genes. Cell type annotation was

performed as described above and refined using scRNA-seq marker genes identified in adult anterior lateral motor cortex (Tasic et al. 2018) (http://celltypes.brain-map.org/rnaseq/mouse). Two neuronal clusters (Clusters 2, 7) with enrichment of glial, mitochondrial, and/or ribosomal genes among their marker genes were included in analyses but excluded from data visualizations. Contributions of neurons to each cluster by genotype were compared using Fisher's exact test. We used the Wilcoxon rank sum test to calculate pseudo-bulk RNA-seq differentially expressed genes (DEGs) in two approaches: between genotypes for all neurons or between genotypes within each neuronal cluster. Enrichment of all-neuron DEGs among neuronal cluster markers was analyzed using hypergeometric testing with a background of 2800 genes. Gene ontology (GO) analysis was performed using ToppFun from the ToppGene Suite (Chen et al. 2009), and Biological Process GO categories with Benjamini-Hochberg (BH) FDR<0.05 were summarized and plotted using REVIGO, with allowed similarity=0.5 and GO term database for *Mus musculus* (Supek et al. 2011). To identify putative Foxp2 direct gene targets, we calculated the Spearman correlation coefficients between *Foxp2* and all other genes in control cells, and then overlapped genes with $|\rho|>0.1$ and BH FDR<0.05 with the E16.5 brain Foxp2 ChIP long list from (Vernes et al. 2011).

Gene Expression Omnibus (GEO) accession information

The National Center for Biotechnology Information GEO accession number for the scRNA-seq data reported in this study is XXXXXXXX.

Acknowledgments

Our sincerest thanks to Peter Tsai, Maria Chahrour, Todd Roberts, Jane Johnson, Ashley Anderson, and Ana Ortiz for providing feedback on the manuscript. G.K. is a Jon Heighten Scholar in Autism Research at UT Southwestern. This work was supported by an Autism Science Foundation Predoctoral Fellowship (15-002) and NIH training grants (NIGMS T32GM109776 and NCATS TL1TR001104) to M.C., and the Simons Foundation (SFARI 573689 and 401220), the James S. McDonnell Foundation 21st Century Science Initiative in Understanding Human Cognition – Scholar Award (220020467), the Chan Zuckerberg Initiative, an advised fund of Silicon Valley Community Foundation (HCA-A-1704-01747), and grants from the NIH (DC014702, DC016340, MH102603) to G.K. We would like to thank Dr. Shari Birnbaum at the UT Southwestern Rodent Behavior Core for collecting behavior data and providing helpful discussions. We also thank the Neuroscience Microscopy, Whole Brain Microscopy, and Flow Cytometry Facilities at UT Southwestern.

Author Contributions

M.C. and G.K. designed the study. M.C. collected and analyzed behavior, immunohistochemistry, and scRNA-seq data, and wrote the manuscript. S.L.H. and A.K. performed bioinformatic analyses on scRNA-seq data. M.H. collected behavior data, maintained mouse lines, and performed genotyping.

References

Ade KK, Wan Y, Chen M, Gloss B, Calakos N. 2011. An Improved BAC Transgenic Fluorescent Reporter Line for Sensitive and Specific Identification of Striatonigral Medium Spiny Neurons. *Frontiers in systems neuroscience* **5**: 32.

Anastasiades PG, Boada C, Carter AG. 2018. Cell-Type-Specific D1 Dopamine Receptor Modulation of Projection Neurons and Interneurons in the Prefrontal Cortex. *Cerebral cortex (New York, NY : 1991)*.

Andersen SL, Thompson AT, Rutstein M, Hostetter JC, Teicher MH. 2000. Dopamine receptor pruning in prefrontal cortex during the periadolescent period in rats. *Synapse (New York, NY)* **37**: 167-169.

Andrews S. 2010. FastQC: a quality control tool for high throughput sequence data.

Araujo DJ, Anderson AG, Berto S, Runnels W, Harper M, Ammanuel S, Rieger MA, Huang HC, Rajkovich K, Loerwald KW et al. 2015. FoxP1 orchestration of ASD-relevant signaling pathways in the striatum. *Genes & development* **29**: 2081-2096.

Araujo DJ, Toriumi K, Escamilla CO, Kulkarni A, Anderson AG, Harper M, Usui N, Ellegood J, Lerch JP, Birnbaum SG et al. 2017. Foxp1 in Forebrain Pyramidal Neurons Controls Gene Expression Required for Spatial Learning and Synaptic Plasticity. *The Journal of neuroscience : the official journal of the Society for Neuroscience* **37**: 10917-10931.

Bedogni F, Hodge RD, Elsen GE, Nelson BR, Daza RA, Beyer RP, Bammler TK, Rubenstein JL, Hevner RF. 2010. Tbr1 regulates regional and laminar identity of postmitotic neurons in developing neocortex. *Proceedings of the National Academy of Sciences of the United States of America* **107**: 13129-13134.

Butler A, Hoffman P, Smibert P, Papalexi E, Satija R. 2018. Integrating single-cell transcriptomic data across different conditions, technologies, and species. *Nature biotechnology* **36**: 411-420.

Calaminus C, Hauber W. 2008. Guidance of instrumental behavior under reversal conditions requires dopamine D1 and D2 receptor activation in the orbitofrontal cortex. *Neuroscience* **154**: 1195-1204.

Castellucci GA, McGinley MJ, McCormick DA. 2016. Knockout of Foxp2 disrupts vocal development in mice. *Scientific reports* **6**: 23305.

Chabout J, Sarkar A, Patel SR, Radden T, Dunson DB, Fisher SE, Jarvis ED. 2016. A Foxp2 Mutation Implicated in Human Speech Deficits Alters Sequencing of Ultrasonic Vocalizations in Adult Male Mice. *Frontiers in behavioral neuroscience* **10**: 197.

Chang J, Gilman SR, Chiang AH, Sanders SJ, Vitkup D. 2015. Genotype to phenotype relationships in autism spectrum disorders. *Nature neuroscience* **18**: 191-198.

Chen J, Bardes EE, Aronow BJ, Jegga AG. 2009. ToppGene Suite for gene list enrichment analysis and candidate gene prioritization. *Nucleic acids research* **37**: W305-311.

Chen YC, Kuo HY, Bornschein U, Takahashi H, Chen SY, Lu KM, Yang HY, Chen GM, Lin JR, Lee YH et al. 2016. Foxp2 controls synaptic wiring of corticostriatal circuits and vocal communication by opposing Mef2c. *Nature neuroscience* **19**: 1513-1522.

Crandall JE, McCarthy DM, Araki KY, Sims JR, Ren JQ, Bhide PG. 2007. Dopamine receptor activation modulates GABA neuron migration from the basal forebrain to the cerebral cortex. *The Journal of neuroscience : the official journal of the Society for Neuroscience* **27**: 3813-3822.

Cui Q, Li Q, Geng H, Chen L, Ip NY, Ke Y, Yung WH. 2018. Dopamine receptors mediate strategy abandoning via modulation of a specific prelimbic cortex-nucleus accumbens pathway in mice. *Proceedings of the National Academy of Sciences of the United States of America* **115**: E4890-e4899.

Demontis D, Walters RK, Martin J, Mattheisen M, Als TD, Agerbo E, Baldursson G, Belliveau R, Bybjerg-Grauholm J, Baekvad-Hansen M et al. 2019. Discovery of the first genome-wide significant risk loci for attention deficit/hyperactivity disorder. *Nature genetics* **51**: 63-75.

Deriziotis P, O'Roak BJ, Graham SA, Estruch SB, Dimitropoulou D, Bernier RA, Gerdts J, Shendure J, Eichler EE, Fisher SE. 2014. De novo TBR1 mutations in sporadic autism disrupt protein functions. *Nature communications* **5**: 4954.

Dobin A, Davis CA, Schlesinger F, Drenkow J, Zaleski C, Jha S, Batut P, Chaisson M, Gingeras TR. 2013. STAR: ultrafast universal RNA-seq aligner. *Bioinformatics (Oxford, England)* **29**: 15-21.

Enard W, Gehre S, Hammerschmidt K, Holter SM, Blass T, Somel M, Bruckner MK, Schreiweis C, Winter C, Sohr R et al. 2009. A humanized version of Foxp2 affects cortico-basal ganglia circuits in mice. *Cell* **137**: 961-971.

Estruch SB, Graham SA, Quevedo M, Vino A, Dekkers DHW, Deriziotis P, Sollis E, Demmers J, Poot RA, Fisher SE. 2018. Proteomic analysis of FOXP proteins reveals interactions between cortical transcription factors associated with neurodevelopmental disorders. *Human molecular genetics*.

Fazel Darbandi S, Robinson Schwartz SE, Qi Q, Catta-Preta R, Pai EL, Mandell JD, Everitt A, Rubin A, Krasnoff RA, Katzman S et al. 2018. Neonatal Tbr1 Dosage Controls Cortical Layer 6 Connectivity. *Neuron* **100**: 831-845.e837.

Floresco SB. 2013. Prefrontal dopamine and behavioral flexibility: shifting from an "inverted-U" toward a family of functions. *Front Neurosci* **7**: 62.

French CA, Fisher SE. 2014. What can mice tell us about Foxp2 function? *Current opinion in neurobiology* **28**: 72-79.

French CA, Groszer M, Preece C, Coupe AM, Rajewsky K, Fisher SE. 2007. Generation of mice with a conditional Foxp2 null allele. *Genesis (New York, NY : 2000)* **45**: 440-446.

French CA, Vinueza Veloz MF, Zhou K, Peter S, Fisher SE, Costa RM, De Zeeuw CI. 2018. Differential effects of Foxp2 disruption in distinct motor circuits. *Molecular psychiatry* **24**: 447-462.

Fujita-Jimbo E, Momoi T. 2014. Specific expression of FOXP2 in cerebellum improves ultrasonic vocalization in heterozygous but not in homozygous Foxp2 (R552H) knock-in pups. *Neuroscience letters* **566**: 162-166.

Gaspar P, Bloch B, Le Moine C. 1995. D1 and D2 receptor gene expression in the rat frontal cortex: cellular localization in different classes of efferent neurons. *The European journal of neuroscience* **7**: 1050-1063.

Gaub S, Fisher SE, Ehret G. 2016. Ultrasonic vocalizations of adult male Foxp2-mutant mice: behavioral contexts of arousal and emotion. *Genes, brain, and behavior* **15**: 243-259.

Gaub S, Groszer M, Fisher SE, Ehret G. 2010. The structure of innate vocalizations in Foxp2-deficient mouse pups. *Genes, brain, and behavior* **9**: 390-401.

Ghirardi L, Brikell I, Kuja-Halkola R, Freitag CM, Franke B, Asherson P, Lichtenstein P, Larsson H. 2017. The familial co-aggregation of ASD and ADHD: a register-based cohort study. *Molecular psychiatry* **23**: 257.

Goebbels S, Bormuth I, Bode U, Hermanson O, Schwab MH, Nave KA. 2006. Genetic targeting of principal neurons in neocortex and hippocampus of NEX-Cre mice. *Genesis (New York, NY : 2000)* **44**: 611-621.

Gorski JA, Talley T, Qiu M, Puelles L, Rubenstein JL, Jones KR. 2002. Cortical excitatory neurons and glia, but not GABAergic neurons, are produced in the Emx1-expressing lineage. *The Journal of neuroscience : the official journal of the Society for Neuroscience* **22**: 6309-6314.

Groszer M, Keays DA, Deacon RM, de Bono JP, Prasad-Mulcare S, Gaub S, Baum MG, French CA, Nicod J, Coventry JA et al. 2008. Impaired synaptic plasticity and motor learning in mice with a point mutation implicated in human speech deficits. *Current biology : CB* **18**: 354-362.

Han SW, Kim YC, Narayanan NS. 2017. Projection targets of medial frontal D1DR-expressing neurons. *Neuroscience letters* **655**: 166-171.

Hickey SL, Berto S, Konopka G. 2019. Chromatin decondensation by FOXP2 promotes human neuron maturation and expression of neurodevelopmental disease genes. *Cell reports*: In press.

Hisaoka T, Nakamura Y, Senba E, Morikawa Y. 2010. The forkhead transcription factors, Foxp1 and Foxp2, identify different subpopulations of projection neurons in the mouse cerebral cortex. *Neuroscience* **166**: 551-563.

Holy TE, Guo Z. 2005. Ultrasonic songs of male mice. *PLoS biology* **3**: e386.

Huang TN, Chuang HC, Chou WH, Chen CY, Wang HF, Chou SJ, Hsueh YP. 2014. Tbr1 haploinsufficiency impairs amygdalar axonal projections and results in cognitive abnormality. *Nature neuroscience* **17**: 240-247.

Jacobs EC, Campagnoni C, Kampf K, Reyes SD, Kalra V, Handley V, Xie YY, Hong-Hu Y, Spreur V, Fisher RS et al. 2007. Visualization of corticofugal projections during early cortical development in a tau-GFP-transgenic mouse. *The European journal of neuroscience* **25**: 17-30.

Kent WJ, Sugnet CW, Furey TS, Roskin KM, Pringle TH, Zahler AM, Haussler D. 2002. The human genome browser at UCSC. *Genome research* **12**: 996-1006.

Konopka G, Roberts TF. 2016. Insights into the Neural and Genetic Basis of Vocal Communication. *Cell* **164**: 1269-1276.

Lalonde R. 2002. The neurobiological basis of spontaneous alternation. *Neuroscience and biobehavioral reviews* **26**: 91-104.

Liao Y, Smyth GK, Shi W. 2014. featureCounts: an efficient general purpose program for assigning sequence reads to genomic features. *Bioinformatics (Oxford, England)* **30**: 923-930.

Lim L, Mi D, Llorca A, Marin O. 2018. Development and Functional Diversification of Cortical Interneurons. *Neuron* **100**: 294-313.

Liu J, Wang F, Huang C, Long LH, Wu WN, Cai F, Wang JH, Ma LQ, Chen JG. 2009. Activation of phosphatidylinositol-linked novel D1 dopamine receptor contributes to the calcium mobilization in cultured rat prefrontal cortical astrocytes. *Cellular and molecular neurobiology* **29**: 317-328.

Loo L, Simon JM, Xing L, McCoy ES, Niehaus JK, Guo J, Anton ES, Zylka MJ. 2019. Single-cell transcriptomic analysis of mouse neocortical development. *Nature communications* **10**: 134.

Medvedeva VP, Rieger MA, Vieth B, Mombereau C, Ziegenhain C, Ghosh T, Cressant A, Enard W, Granon S, Dougherty JD et al. 2018. Altered social behavior in mice carrying a cortical Foxp2 deletion. *Human molecular genetics*.

Mizoguchi K, Shoji H, Tanaka Y, Maruyama W, Tabira T. 2009. Age-related spatial working memory impairment is caused by prefrontal cortical dopaminergic dysfunction in rats. *Neuroscience* **162**: 1192-1201.

Mizoguchi K, Shoji H, Tanaka Y, Tabira T. 2010. Orbitofrontal dopaminergic dysfunction causes age-related impairment of reversal learning in rats. *Neuroscience* **170**: 1110-1119.

Molyneaux BJ, Goff LA, Brettler AC, Chen HH, Hrvatin S, Rinn JL, Arlotta P. 2015. DeCoN: genome-wide analysis of in vivo transcriptional dynamics during pyramidal neuron fate selection in neocortex. *Neuron* **85**: 275-288.

Money KM, Stanwood GD. 2013. Developmental origins of brain disorders: roles for dopamine. *Frontiers in cellular neuroscience* **7**: 260.

Morgan A, Fisher SE, Scheffer I, Hildebrand M. 2017. FOXP2-Related Speech and Language Disorders. in *GeneReviews((R))* (eds. MP Adam, HH Ardinger, RA Pagon, SE Wallace, LJH Bean, K Stephens, A Amemiya). University of Washington, Seattle

University of Washington, Seattle. GeneReviews is a registered trademark of the University of Washington, Seattle. All rights reserved., Seattle (WA).

Murugan M, Harward S, Scharff C, Mooney R. 2013. Diminished FoxP2 levels affect dopaminergic modulation of corticostriatal signaling important to song variability. *Neuron* **80**: 1464-1476.

Nakayama H, Ibanez-Tallon I, Heintz N. 2018. Cell-Type-Specific Contributions of Medial Prefrontal Neurons to Flexible Behaviors. *The Journal of neuroscience : the official journal of the Society for Neuroscience* **38**: 4490-4504.

Portmann T, Yang M, Mao R, Panagiotakos G, Ellegood J, Dolen G, Bader PL, Grueter BA, Goold C, Fisher E et al. 2014. Behavioral abnormalities and circuit defects in the basal ganglia of a mouse model of 16p11.2 deletion syndrome. *Cell reports* **7**: 1077-1092.

Reuter MS, Riess A, Moog U, Briggs TA, Chandler KE, Rauch A, Stampfer M, Steindl K, Glaser D, Joset P et al. 2017. FOXP2 variants in 14 individuals with developmental speech and language disorders broaden the mutational and clinical spectrum. *Journal of medical genetics* **54**: 64-72.

Rieger MA, Dougherty JD. 2016. Analysis of within Subjects Variability in Mouse Ultrasonic Vocalization: Pups Exhibit Inconsistent, State-Like Patterns of Call Production. *Frontiers in behavioral neuroscience* **10**: 182.

Robinson JE, Gradinaru V. 2018. Dopaminergic dysfunction in neurodevelopmental disorders: recent advances and synergistic technologies to aid basic research. *Current opinion in neurobiology* **48**: 17-29.

Satterstrom FK Kosmicki JA Wang J Breen MS De Rubeis S An J-Y Peng M Collins RL Grove J Klei L et al. 2019. Large-scale exome sequencing study implicates both developmental and functional changes in the neurobiology of autism. *bioRxiv*: 484113.

Schreiweis C, Bornschein U, Burguiere E, Kerimoglu C, Schreiter S, Dannemann M, Goyal S, Rea E, French CA, Puliyadi R et al. 2014. Humanized Foxp2

accelerates learning by enhancing transitions from declarative to procedural performance. *Proceedings of the National Academy of Sciences of the United States of America* **111**: 14253-14258.

Schulze K, Vargha-Khadem F, Mishkin M. 2017. Phonological working memory and FOXP2. *Neuropsychologia* **108**: 147-152.

Shu W, Cho JY, Jiang Y, Zhang M, Weisz D, Elder GA, Schmeidler J, De Gasperi R, Sosa MA, Rabidou D et al. 2005. Altered ultrasonic vocalization in mice with a disruption in the Foxp2 gene. *Proceedings of the National Academy of Sciences of the United States of America* **102**: 9643-9648.

Sia GM, Clem RL, Huganir RL. 2013. The human language-associated gene SRPX2 regulates synapse formation and vocalization in mice. *Science (New York, NY)* **342**: 987-991.

Smith T, Heger A, Sudbery I. 2017. UMI-tools: modeling sequencing errors in Unique Molecular Identifiers to improve quantification accuracy. *Genome research* **27**: 491-499.

Sohur US, Padmanabhan HK, Kotchetkov IS, Menezes JRL, Macklis JD. 2014. Anatomic and molecular development of corticostriatal projection neurons in mice. *Cerebral cortex (New York, NY : 1991)* **24**: 293-303.

Sorensen SA, Bernard A, Menon V, Royall JJ, Glattfelder KJ, Desta T, Hirokawa K, Mortrud M, Miller JA, Zeng H et al. 2015. Correlated gene expression and target specificity demonstrate excitatory projection neuron diversity. *Cerebral cortex (New York, NY : 1991)* **25**: 433-449.

Stoodley CJ, D'Mello AM, Ellegood J, Jakkamsetti V, Liu P, Nebel MB, Gibson JM, Kelly E, Meng F, Cano CA et al. 2017. Altered cerebellar connectivity in autism and cerebellar-mediated rescue of autism-related behaviors in mice. *Nature neuroscience* **20**: 1744-1751.

Supek F, Bosnjak M, Skunca N, Smuc T. 2011. REVIGO summarizes and visualizes long lists of gene ontology terms. *PloS one* **6**: e21800.

Tasic B, Menon V, Nguyen TN, Kim TK, Jarsky T, Yao Z, Levi B, Gray LT, Sorensen SA, Dolbeare T et al. 2016. Adult mouse cortical cell taxonomy revealed by single cell transcriptomics. *Nature neuroscience* **19**: 335-346.

Tasic B, Yao Z, Graybuck LT, Smith KA, Nguyen TN, Bertagnolli D, Goldy J, Garren E, Economo MN, Viswanathan S et al. 2018. Shared and distinct transcriptomic cell types across neocortical areas. *Nature* **563**: 72-78.

Tsui D, Vessey JP, Tomita H, Kaplan DR, Miller FD. 2013. FoxP2 regulates neurogenesis during embryonic cortical development. *The Journal of neuroscience : the official journal of the Society for Neuroscience* **33**: 244-258.

Usui N, Araujo DJ, Kulkarni A, Co M, Ellegood J, Harper M, Toriumi K, Lerch JP, Konopka G. 2017a. Foxp1 regulation of neonatal vocalizations via cortical development. *Genes & development* **31**: 2039-2055.

Usui N, Co M, Harper M, Rieger MA, Dougherty JD, Konopka G. 2017b. Sumoylation of FOXP2 Regulates Motor Function and Vocal Communication Through Purkinje Cell Development. *Biological psychiatry* **81**: 220-230.

Van Segbroeck M, Knoll AT, Levitt P, Narayanan S. 2017. MUPET-Mouse Ultrasonic Profile ExTraction: A Signal Processing Tool for Rapid and Unsupervised Analysis of Ultrasonic Vocalizations. *Neuron* **94**: 465-485.e465.

Vernes SC, Oliver PL, Spiteri E, Lockstone HE, Puliyadi R, Taylor JM, Ho J, Mombereau C, Brewer A, Lowy E et al. 2011. Foxp2 regulates gene networks implicated in neurite outgrowth in the developing brain. *PLoS genetics* **7**: e1002145.

Vincent SL, Khan Y, Benes FM. 1993. Cellular distribution of dopamine D1 and D2 receptors in rat medial prefrontal cortex. *The Journal of neuroscience : the official journal of the Society for Neuroscience* **13**: 2551-2564.

Willsey AJ, Sanders SJ, Li M, Dong S, Tebbenkamp AT, Muhle RA, Reilly SK, Lin L, Fertuzinhos S, Miller JA et al. 2013. Coexpression networks implicate human midfetal deep cortical projection neurons in the pathogenesis of autism. *Cell* **155**: 997-1007.

Xu S, Liu P, Chen Y, Chen Y, Zhang W, Zhao H, Cao Y, Wang F, Jiang N, Lin S et al. 2018. Foxp2 regulates anatomical features that may be relevant for vocal behaviors and bipedal locomotion. *Proceedings of the National Academy of Sciences*.

Yang M, Lewis FC, Sarvi MS, Foley GM, Crawley JN. 2015. 16p11.2 Deletion mice display cognitive deficits in touchscreen learning and novelty recognition tasks. *Learning & memory (Cold Spring Harbor, NY)* **22**: 622-632.

Zheng GX, Terry JM, Belgrader P, Ryvkin P, Bent ZW, Wilson R, Ziraldo SB, Wheeler TD, McDermott GP, Zhu J et al. 2017. Massively parallel digital transcriptional profiling of single cells. *Nature communications* **8**: 14049.

Co_Table 1

Layer 5												
	% DAPI+…			% Foxp2+…			% tdTom+…			% TLE4+…		
	CTL	CKO	Pval	CTL	CKO	Pval	CTL	CKO	Pval	CTL	CKO	Pval
…also Foxp2+	14 ± 1.1	-	-	-	-	-	28 ± 5.3	-	-	62 ± 2.1	-	-
…also tdTom+	33 ± 3.2	14 ± 2.8	**0.0213**	63 ± 1.4	-	-	-	-	-	100 ± 0.0	30 ± 6.4	**0.0035**
…also TLE4+	8.8 ± 1.7	8.3 ± 0.7	0.7605	38 ± 3.5	-	-	28 ± 8.0	19 ± 1.8	0.2504	-	-	-
…Foxp2+tdTom+TLE4+	5.5 ± 0.9	-	-									
…Foxp2+tdTom+TLE4-	3.4 ± 0.04	-	-									
…Foxp2+tdTom-TLE4+	0.0 ± 0.0	-	-									
…Foxp2+tdTom-TLE4-	5.2 ± 0.2	-	-									
…tdTom+TLE4+	8.8 ± 1.7	2.5 ± 0.6	**0.0244**									
…tdTom+TLE4-	24 ± 4.9	11 ± 2.3	0.0735									
…tdTom-TLE4+	0.0 ± 0.0	5.8 ± 0.6	**0.0062**									

Layer 6												
	% DAPI+…			% Foxp2+…			% tdTom+…			% TLE4+…		
	CTL	CKO	Pval	CTL	CKO	Pval	CTL	CKO	Pval	CTL	CKO	Pval
…also Foxp2+	52 ± 3.3	-	-	-	-	-	79 ± 0.7	-	-	93 ± 1.6	-	-
…also tdTom+	66 ± 3.9	25 ± 1.5	**0.0014**	99 ± 1.1	-	-	-	-	-	99 ± 0.8	41 ± 3.2	**0.0008**
…also TLE4+	35 ± 1.7	32 ± 2.4	0.4326	62 ± 0.2	-	-	53 ± 1.1	53 ± 3.6	0.9069	-	-	-
…Foxp2+tdTom+TLE4+	32 ± 1.8	-	-									
…Foxp2+tdTom+TLE4-	20 ± 0.8	-	-									
…Foxp2+tdTom-TLE4+	0.3 ± 0.3	-	-									
…Foxp2+tdTom-TLE4-	0.5 ± 0.3	-	-									
…tdTom+TLE4+	34 ± 1.4	13 ± 0.2	**0.0003**									
…tdTom+TLE4-	31 ± 2.6	12 ± 1.6	**0.0061**									
…tdTom-TLE4+	0.3 ± 0.3	19 ± 2.3	**0.0088**									

Table 1. Summary of Foxp2, tdTomato, and TLE4 coexpression in P7 mPFC layers 5 and 6. Data are represented as means±SEM. Genotypes were compared using t-tests. *n* = 2-3 per condition.

Co_Fig1

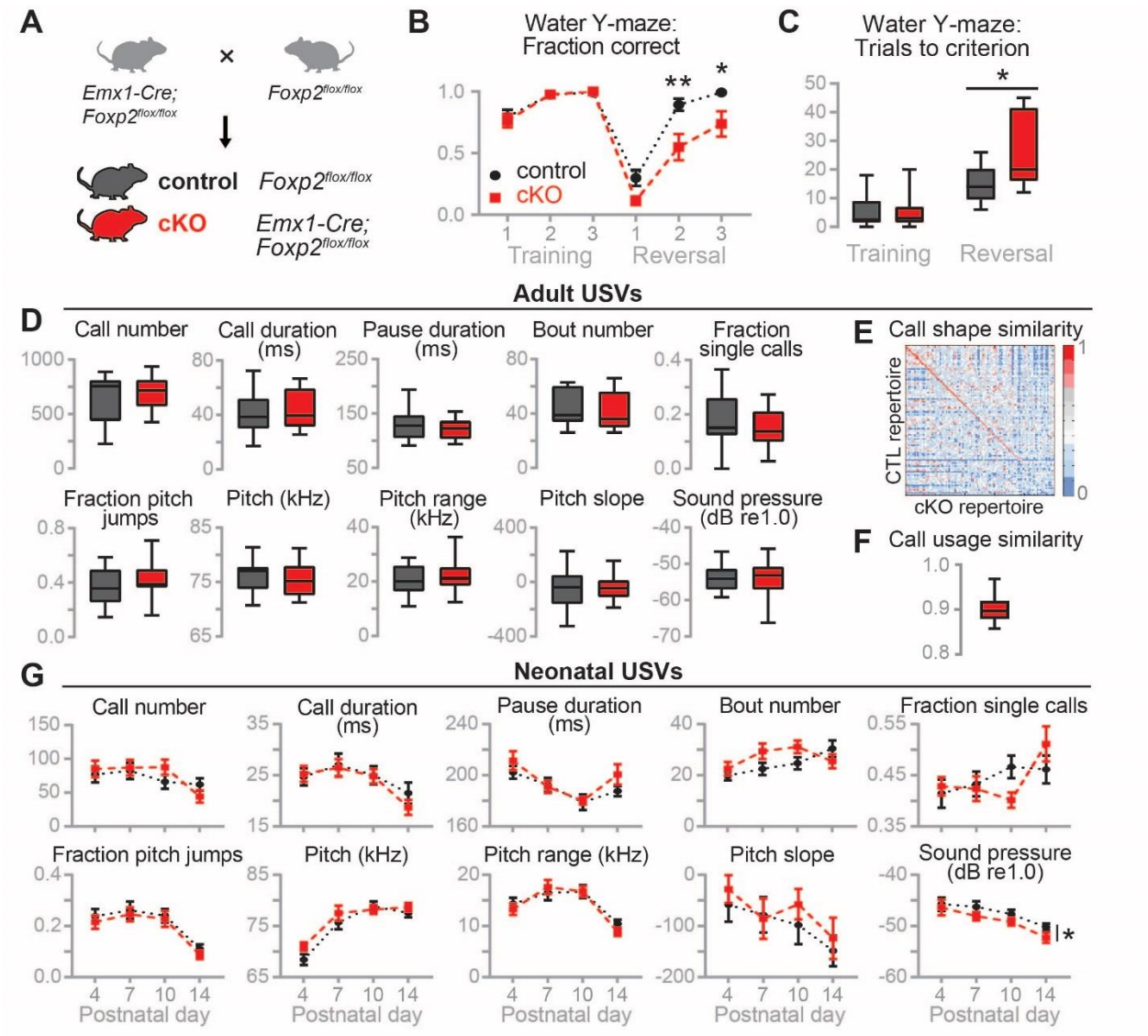

Figure 1. *Foxp2* cKO mice show behavioral inflexibility but normal vocalizations. (A) Breeding scheme to generate control (*Foxp2*$^{flox/flox}$) and *Foxp2* cKO (*Emx1-Cre; Foxp2*$^{flox/flox}$) littermate mice. (B-C) Reversal learning in water Y-maze. *n* = 10-17 per condition. (B) Fraction of correct trials. Data are shown as means (±SEM). (*) $P < 0.05$, (**) $P < 0.01$, two-way ANOVA with Bonferroni's multiple comparisons test. (C) Number of trials to criterion. Box shows 25-75 percentiles, whiskers show min-max. (*) $P < 0.05$, t-test. (D-G) Analysis of USVs. (D) Adult courtship USVs. Box shows 25-75 percentiles, whiskers show min-max. *n* = 14-15 per condition. (E) Call shape similarity matrix between adult control and cKO USV repertoires (size 100). Scale represents Pearson correlation coefficient. (F) Call usage similarity of adult cKOs compared to controls. Box shows 25-75 percentiles, whiskers show 5-95 percentiles. (G) Neonatal isolation USVs. Data are represented as means (±SEM). (*) $P < 0.05$, two-way ANOVA with Bonferroni's multiple

comparisons test. *n* = 34-42 per condition. Full statistical analysis can be found in Supplemental Table 1.

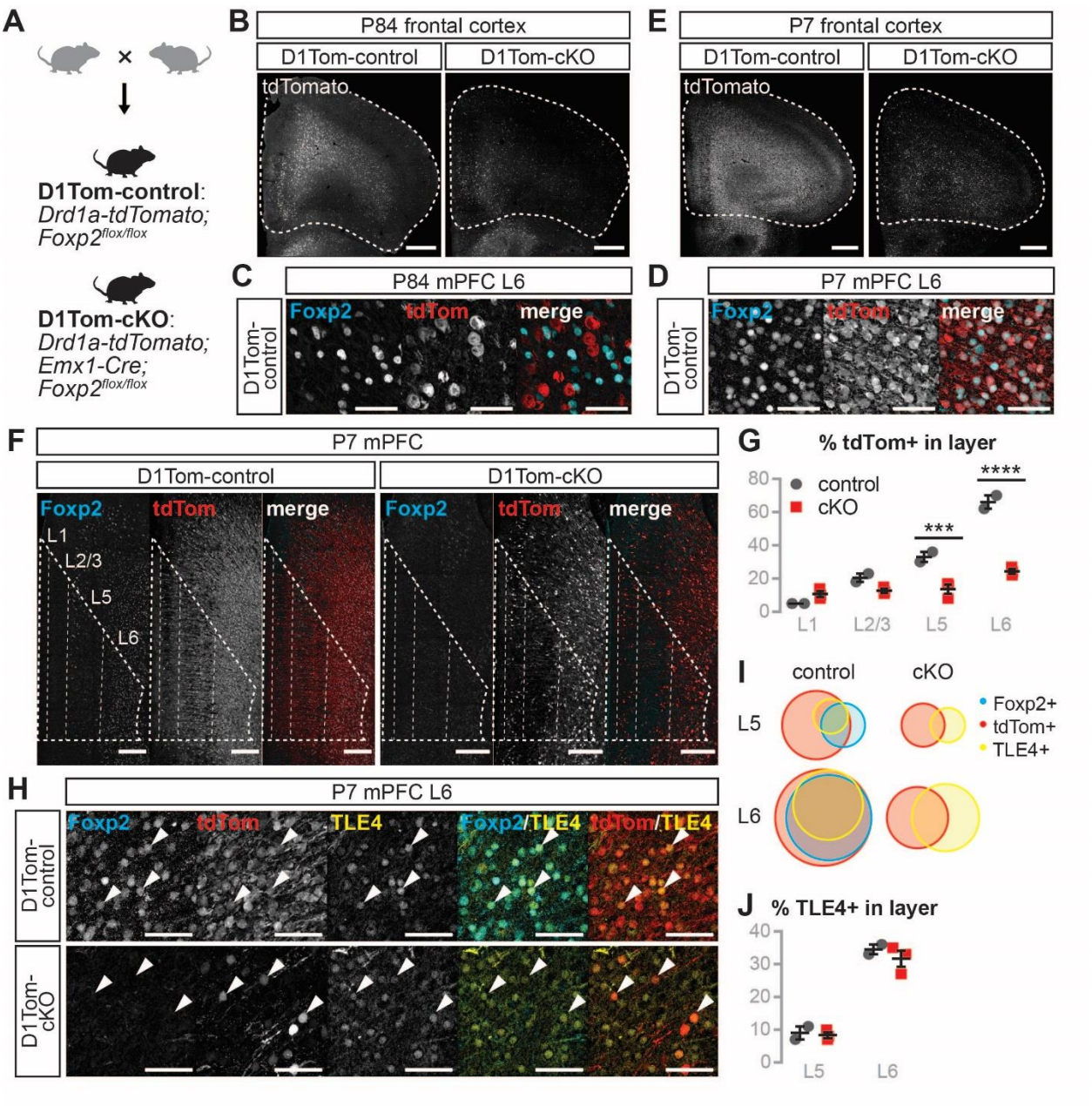

Figure 2. *Foxp2* cKO mice show decreased dopamine D1 receptor expression in postnatal and adult cortex. (A) Breeding scheme to generate control and cKO littermate mice expressing *Drd1a*-tdTomato. (B) Immunohistochemistry (IHC) for tdTomato in adult control and cKO frontal cortex. Scale bar: 500 µm. (C) IHC for Foxp2 and tdTomato in adult control mPFC L6. Scale bar: 50 µm. (D) IHC for Foxp2 and tdTomato in P7 control mPFC L6. Scale bar: 50 µm. (E) IHC for tdTomato in P7 control and cKO frontal cortex. Scale bar: 500 µm. (F) IHC for Foxp2 and tdTomato in P7 control and cKO mPFC. Scale bar: 200 µm. (G) Percentage of DAPI+ cells expressing tdTomato per layer in P7 mPFC. Error bars represent ±SEM. (***) $P < 0.001$, (****) $P < 0.0001$, two-way ANOVA with

Bonferroni's multiple comparisons test. *n* = 2-3 per condition. Full statistical analysis can be found in Supplemental Table 1. (H) IHC for Foxp2, tdTomato, and TLE4 in P7 control and cKO mPFC L6. Arrowheads indicate cells with protein coexpression. Scale bar: 50 µm. (I) Summary Venn diagrams of Foxp2, tdTomato, and TLE4 coexpression in P7 control and cKO mPFC L5 and L6. (J) Percentage of DAPI+ cells expressing TLE4 in P7 control and cKO mPFC L5 and L6. Error bars represent ±SEM. Quantification and statistical analysis for I-J can be found in Table 1.

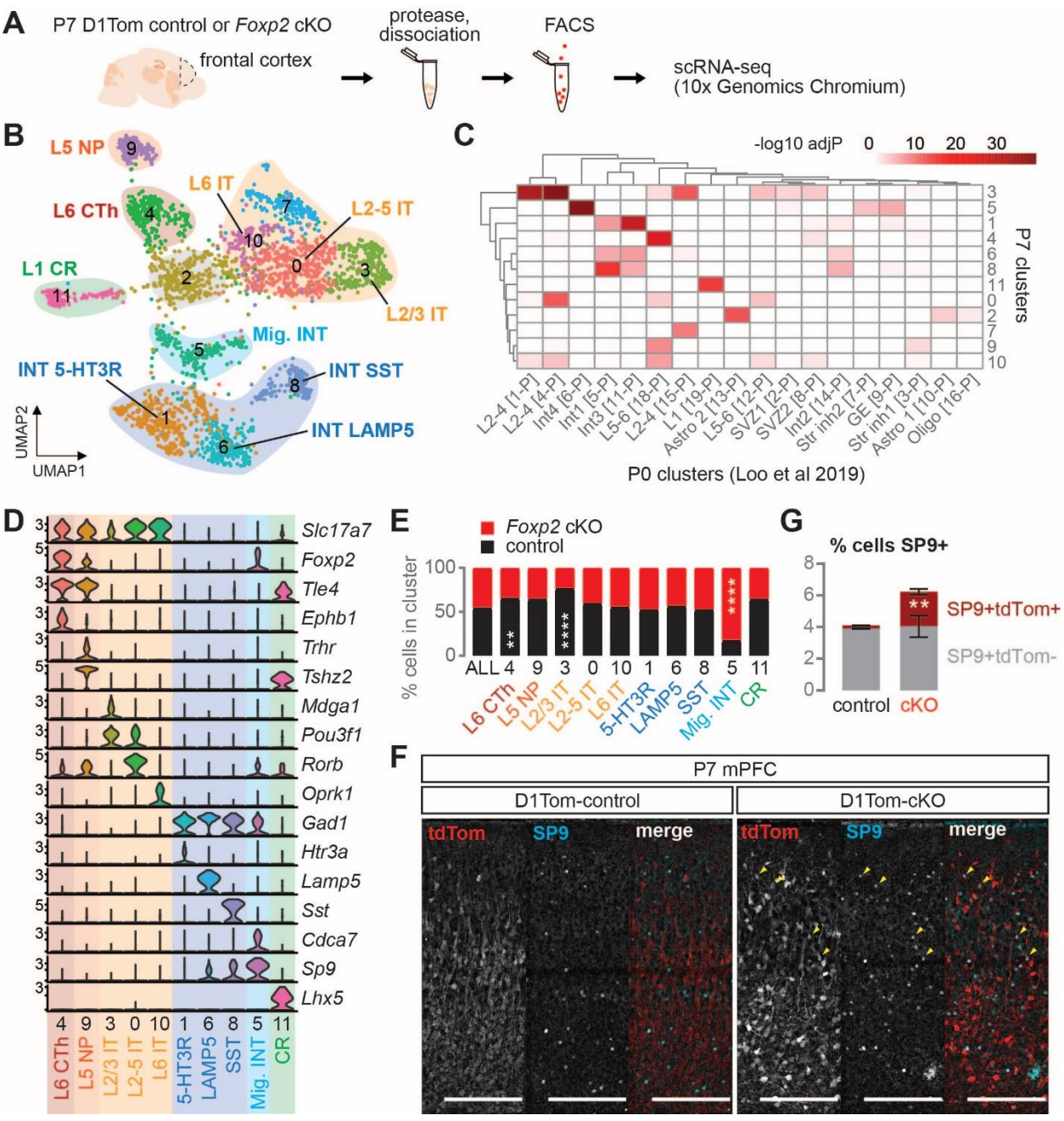

Figure 3. *Foxp2* cKO mice show altered composition of dopamine D1 receptor-expressing neuronal subtypes. (A) Experimental design. *n* = 2 per condition. (B) UMAP projection of clusters with neurons combined from both genotypes. (C) Hypergeometric overlaps of neuronal cluster marker genes with P0 mouse cortex cluster marker genes from Loo et al 2019. (D) Violin plots of selected marker genes. Y-axes show log-scaled expression. (E) Percentage of control and cKO cells per cluster. (**) $P < 0.01$, (****) $P < 0.0001$, Fisher's exact test with Benjamini-Hochberg post-hoc test. (F) IHC for tdTomato and SP9 in P7 control and cKO mPFC. Pial surface is at the top. Arrowheads indicate

cells expressing both proteins. Scale bar: 200 µm. (G) Percentage of cells expressing SP9 ± tdTomato in P7 control and cKO mPFC. Data are represented as means±SEM. (**) $P < 0.01$, t-test. CR: Cajal-Retzius, CTh: corticothalamic, INT: interneuron, IT: intratelencephalic, Mig INT: migrating interneuron, NP: near-projecting.

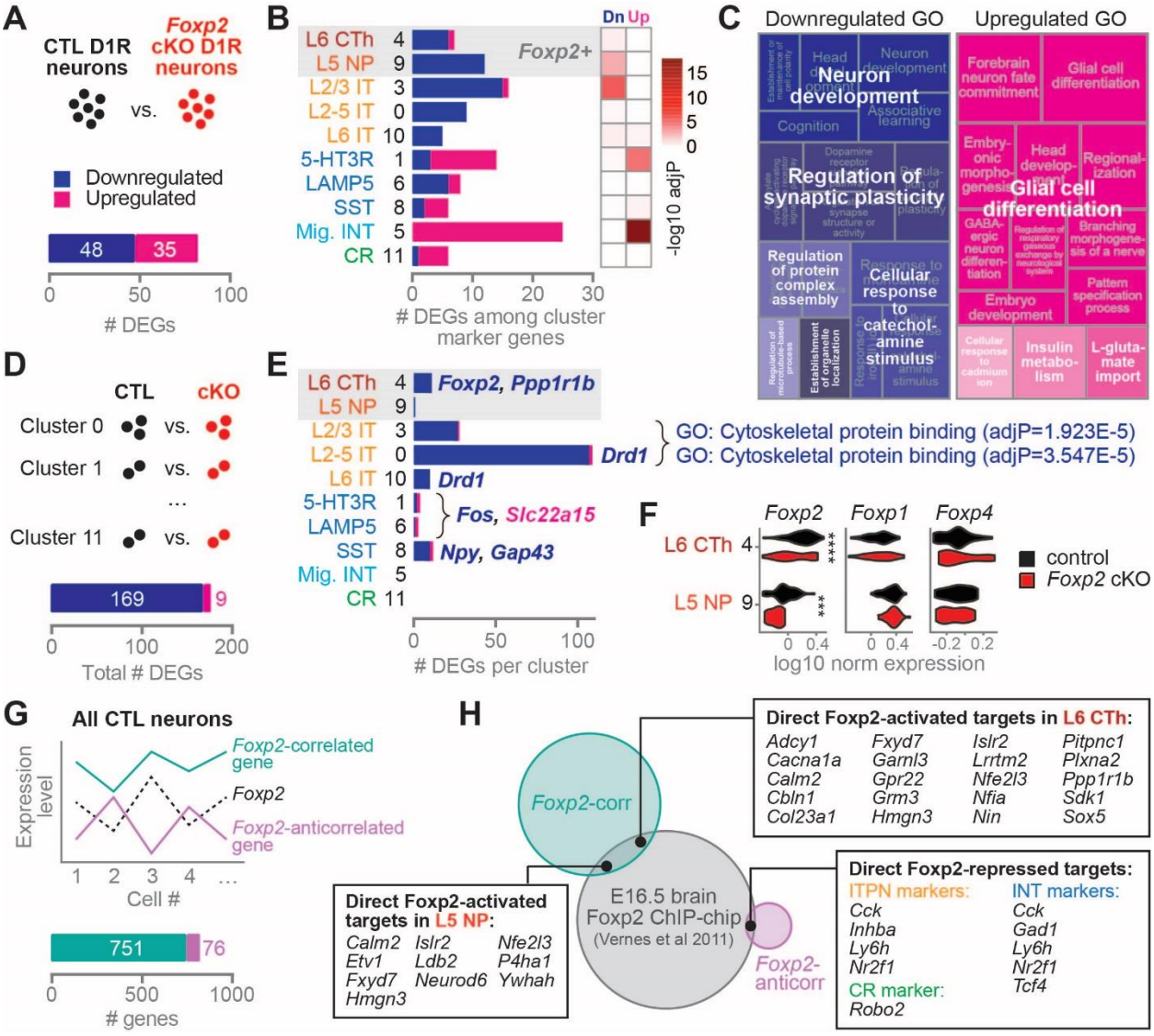

Figure 4. Identification of cell-autonomous and non-cell-autonomous gene expression programs regulated by cortical Foxp2. (A-C) Differential gene expression analyses between all control and all *Foxp2* cKO neurons. (A) Number of DEGs significantly down- or upregulated in cKO neurons. (B) Number (left) and hypergeometric enrichment (right) of DEGs among neuronal cluster marker genes. Shaded area indicates clusters with *Foxp2* enrichment. (C) Treemaps of summarized gene ontology biological process terms for down- and upregulated DEGs. (D-E) Analysis of DEGs by cluster between control and cKO neurons. (D) Total number of DEGs down- or upregulated in cKO neurons. (E) Number of DEGs per cluster with selected genes and gene ontology terms. Shaded area indicates clusters with *Foxp2* enrichment. (F) Violin plots of *Foxp* gene expression in clusters with *Foxp2* enrichment. (***) $P < 0.001$, (****) $P < 0.0001$, Wilcoxon rank sum test. (G-H) Analysis of genes correlated or anticorrelated with *Foxp2* expression across control neurons. (G) Number of *Foxp2*-correlated or -anticorrelated

genes. (H) Overlap of *Foxp2*-correlated or -anticorrelated genes with embryonic brain Foxp2 ChIP-chip targets from (Vernes et al. 2011) and with neuronal cluster marker genes.

Co_Fig5

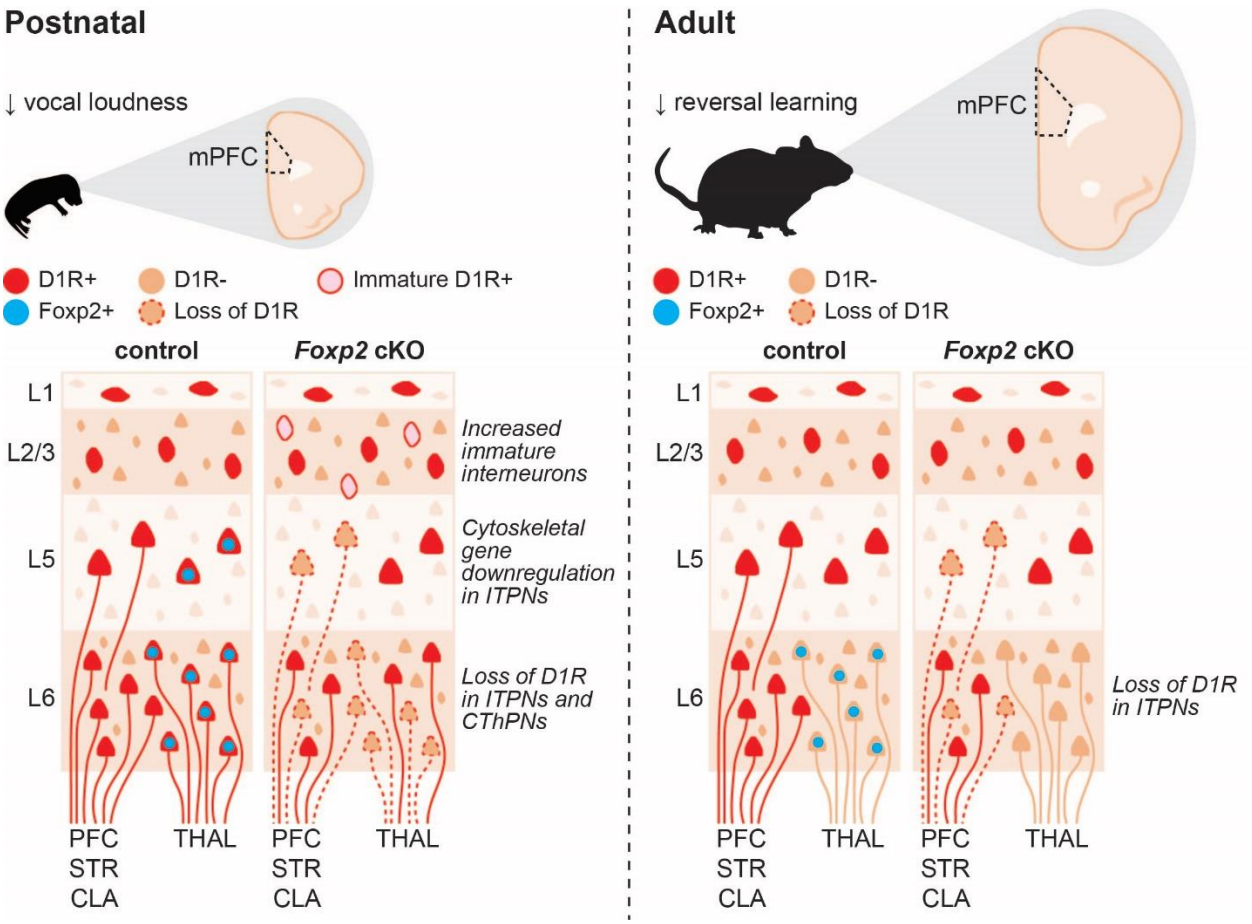

Figure 5. Summary of findings in *Foxp2* cKO postnatal and adult mice. CLA: claustrum, CThPNs: corticothalamic projection neurons, D1R: dopamine D1 receptor, ITPNs: intratelencephalic projection neurons, L: layer, mPFC: medial prefrontal cortex, STR: striatum, THAL: thalamus.